

Selfconsistent description of vector-mesons in matter¹

Felix Riek² and Jörn Knoll³

*Gesellschaft für Schwerionenforschung
Planckstr. 1
64291 Darmstadt*

Abstract

We study the influence of the virtual pion cloud in nuclear matter at finite densities and temperatures on the structure of the ρ - and ω -mesons. The in-matter spectral function of the pion is obtained within a selfconsistent scheme of coupled Dyson equations where the coupling to the nucleon and the $\Delta(1232)$ -isobar resonance is taken into account. The selfenergies are determined using a two-particle irreducible (2PI) truncation scheme (Φ -derivable approximation) supplemented by Migdal's short range correlations for the particle-hole excitations. The so obtained spectral function of the pion is then used to calculate the in-medium changes of the vector-meson spectral functions. With increasing density and temperature a strong interplay of both vector-meson modes is observed. The four-transversality of the polarisation tensors of the vector-mesons is achieved by a projector technique. The resulting spectral functions of both vector-mesons and, through vector dominance, the implications of our results on the dilepton spectra are studied in their dependence on density and temperature.

Key words:

rho-meson, omega-meson, medium modifications, dilepton production, self-consistent approximation schemes.

PACS: 14.40.-n

¹ Supported in part by the Helmholtz Association under Grant No. VH-VI-041

² e-mail:f.riek@gsi.de

³ e-mail:j.knoll@gsi.de

1 Introduction

It is an interesting question how the behaviour of hadrons changes in a dense hadronic medium. One of the driving ideas is that chiral symmetry is expected to become partially restored with increasing density or temperature. Therefore the spectral functions of hadrons in their dependence on the thermodynamic parameters of the hadronic environment are of special interest. They directly show the possible effects on the mass and decay properties of the particles. One of the experimental accesses to observe the spectral functions in-matter is provided through the study of electron-positron- or muon anti-muon pairs, called dileptons [1–5] both in hadron–nucleus and nucleus–nucleus collisions. The advantage of such electromagnetic probes instead of strong interacting particles, like pions or kaons, is that one gets information directly from the centre of the interaction zone. Above invariant masses of 400 MeV the pairs are mainly produced through the decay of vector-mesons like the ρ - and ω -meson. Additional contributions come from bremsstrahlung and final-state Dalitz-decays of other resonances, like the η -meson, which in part are controlled by other observations. Presently all nuclear collision experiments [2–5] observe a significantly enhanced dilepton yield in the invariant mass range below the light vector-meson masses compared to straight extrapolations from elementary processes, like proton-proton scattering. Several mechanisms, especially a lowering of the ρ -meson mass or an increase of its damping width, were proposed to explain the experimental facts [8–29]. Additional experiments for photo-production off nuclei are planned, where one likes to investigate the $\omega \rightarrow \pi^0\gamma \rightarrow 3\gamma$ channel [6,7]. Despite the perturbation through the final state interaction of the π^0 -meson [6] it will still be possible to isolate the ω -meson component because the competing ρ -meson process is highly suppressed.

Ever since the early considerations of vector-mesons in dense matter [30,31,18] much effort has been devoted to study the properties of the ρ -meson, which strongly couples to the two-pion channel. However, with a few exceptions, e.g. [10,12,13], the in-medium properties of the pion are commonly neglected, just employing unperturbed free pion states. Furthermore so far there are only few attempts to study the in-medium properties of the ω -meson [20–25,32–34]. Thus, a more realistic determination of the in-matter pion cloud permits to investigate the dependence of the vector-meson properties on the various components of the pion spectral function in the medium. Compared to a schematic three level model for the pion modes studied by Wachs [34] we use a scheme of coupled Dyson equations in which the pionic degrees of freedom are modified selfconsistently through the coupling to the nucleon and the $\Delta(1232)$ -resonance. All selfenergies are determined within a truncated two-particle irreducible (2PI) effective action formalism (Φ -functional) in their full dependence on energy and three momentum. This guarantees conservation laws of the theory to be fulfilled on the level of expectation values [36] despite

the approximations employed. From the in-medium spectral function of the pion we are able to calculate the modified spectral functions for the ρ -meson as well as for the ω -meson in the coupled scheme. Thereby the process $\rho \rightarrow \omega + \pi$ leads to a strong interplay between both vector-mesons. In particular the ω -width is very sensitive to the space-like, i.e. low energy component of the pion caused by its coupling to nucleon nucleon-hole states. For a realistic treatment of this component Migdal's short range correlations [37] are important. These RPA-type correlations shift the spectral strength to higher energies, such that pion condensation is prevented. In order to concentrate on the effects due to the modified pion we neglected direct couplings of the vector-mesons to the baryonic currents. The latter have been investigated by several authors [35,8,9], who found a multicomponent structure for the in-medium ρ meson which is yet absent in our approach.

Dealing with vector-mesons requires to consider current conservation on the correlator level. This is ensured by a projector formalism [38] which constructs a four-transversal polarisation tensor.

The paper is organised in the following way: We first summarise the essential definitions in the realtime formalism used in the calculations at finite temperature and density. Then we present the model for the in-medium pion coupled to the the baryonic degrees of freedom. Afterwards we show how to derive a four-transversal and thus a current conserving polarisation tensor by means of a projector formalism. For the so obtained in-medium spectral functions of the vector-mesons we use the vector-dominance concept in order to calculate the effect of our results on the dilepton rates. The different decay contributions as well as the effect of possible mass-shifts of the vector-mesons in the dilepton spectra are investigated. A discussion of our results concludes the paper.

2 Realtime formalism and 2PI generating functional

Interested in all spectral properties as a function of real energies the realtime formalism [39] will be used rather than the Matsubara technique. Within this formalism all two-point functions such as the propagator⁴ or selfenergies take four components, e.g.

$$\begin{aligned} iG^{--}(x, x') &\equiv \langle T \hat{\Psi}(x) \hat{\Psi}^\dagger(x') \rangle & iG^{++}(x, x') &\equiv \langle T^{-1} \hat{\Psi}(x) \hat{\Psi}^\dagger(x') \rangle \\ iG^{+-}(x, x') &\equiv \langle \hat{\Psi}(x) \hat{\Psi}^\dagger(x') \rangle & iG^{-+}(x, x') &\equiv \mp \langle \hat{\Psi}^\dagger(x') \hat{\Psi}(x) \rangle, \end{aligned}$$

⁴ We use units with $c = \hbar = 1$ throughout the paper.

depending on the order of the fermionic (upper sign) or bosonic (lower sign) field operators $\hat{\Psi}(x)$ appearing in the expectation values. The space-time coordinates are denoted by x and x' , the time-, respectively, anti-time-ordering is symbolized by T and T^{-1} . The Dyson equations then become matrix equations with respect to the $\{-, +\}$ labels (placement on the closed time contour).

For a uniform medium in thermal equilibrium one can exploit the standard simplification by going to the space-time Fourier-transformation $x - x' \rightarrow p$ of all quantities, where $p = (p^0, \mathbf{p})$ is the four momentum. Then the coupled Dyson equations simply become algebraic and it is sufficient to solve for the retarded (or advanced) Dyson equation, since all four components can be deduced from this by thermal Fermi-Dirac or Bose-Einstein factors arising from the Kubo-Martin-Schwinger (KMS) condition. Thereby the retarded and advanced Green functions follow from

$$\begin{aligned} G^R(p) &\equiv G^{--}(p) - G^{-+}(p) = G^{+-}(p) - G^{++}(p) \\ G^A(p) &\equiv G^{--}(p) - G^{+-}(p) = G^{-+}(p) - G^{++}(p) \\ G^A(p) &\equiv (G^R(p))^\dagger \end{aligned} \quad (1)$$

with the KMS conditions

$$\begin{aligned} iG^{-+} &\equiv \mp n_T(p)A(p) \\ iG^{+-} &\equiv (1 \mp n_T(p))A(p), \end{aligned} \quad (2)$$

where the spectral function and thermal weights are given by

$$\begin{aligned} iA(p) &\equiv G^A(p) - G^R(p) = (G^R(p))^\dagger - G^R(p) \\ n_T(p) &\equiv \frac{1}{\exp((p^0 - \mu)/T) \pm 1} \end{aligned} \quad (3)$$

with temperature T , chemical potential μ and the energy p^0 . The above listed relations for G likewise apply for all equilibrium two-point functions, i.e. also for the selfenergies. They are also written in a way that they apply to Dirac spinors or vector fields, whereby all quantities additionally become Dirac-matrix or Lorentz-tensor structures, respectively. The adjungation denoted by the \dagger -symbol refers to this matrix structure⁵. For relativistic bosons the spectral functions $A(p)$ are normalised to 2π with respect to the integration measure $p^0 dp^0$.

The propagators and selfenergies of the baryons are denoted by G and Σ , while we use D and Π for the corresponding quantities for the meson fields. In selfconsistent two-particle irreducible (2PI) approximation schemes [36,40] the selfenergies Σ or Π for the baryons and mesons are derived from a generating

⁵ Dirac spinors need to be treated with special care since one has to employ the “hermitian” form $\gamma^0 \gamma^\mu$ of the Gamma-matrices before executing the adjungation.

functional, called Φ -functional. This functional is given by a truncated set of closed diagrams in accordance with the interaction Lagrangian where all lines denote dressed, i.e. selfconsistent propagators. The selfenergies result as functional variations with respect to the propagators, i.e.

$$-i\Sigma(x, y) = \frac{\delta i\Phi[G, D]}{\delta iG(y, x)} \quad \text{or} \quad -i\Pi(x, y) = \frac{\delta i\Phi[G, D]}{\delta iD(y, x)}. \quad (4)$$

This implies an opening of a corresponding propagator line in the diagrams of Φ . For the resulting set of coupled Dyson equations such 2PI approaches guarantee that even in a partial resummation of a single class of diagrams the conservation laws which are related to the symmetries of the system are fulfilled on the level of expectation values [36].

3 The Model

The present investigations are restricted to spin as well as isospin symmetric nuclear matter. This implies vanishing chemical potentials for all mesons in the light flavour sector. All selfconsistent calculations of the spectral functions are carried out numerically as a function of energy and momentum on a two dimensional grid of 5 MeV by 5 MeV/c resolution using an iterative procedure. For the model Lagrangian we use the dominant hadron interactions emerging from the low energy chiral limit of QCD, i.e. the Weinberg-Tomozawa couplings[41,42]. Although the fields are not elementary we try to keep the model as free as possible from further ambiguities such as form factors, thus treating most coupling as point-like. Apart from the πNN - and $\pi N\Delta$ -coupling this can be done for all other channels. In no-sea approximation for the baryons all baryon-loops are finite. Loops involving mesons are divergent and would require appropriate regularisation schemes, either in form of a UV-cutoff or by some generalized counter term strategy [43] for some loops up to the 6-point level with corresponding complications [47] for the selfconsistent treatment. Both introduce further ambiguities. In order to circumvent such complications we have dropped the real part of these loops while keeping the normalization of the corresponding spectral functions. The simplification violates the analyticity properties of the selfenergies. However explicit checks showed this of minor importance, in particular for the here addressed vector mesons. For the present investigations we also ignore direct couplings of the vector mesons to the baryonic currents.

3.1 Pions and baryonic Resonances

In the baryon sector the nucleon and the $\Delta(1232)$ -resonance are included. The pion is considered as Goldstone boson of chiral symmetry which, in lowest ap-

proximation in the pion-energy, leads to p -wave couplings to the baryonic pseudo-vector currents together with a minor s -wave term which we ignore. For the energies involved we approximate the spinor structure of the baryons by the non-relativistic limit, while the kinematics is kept in the relativistic form. This approximation allows to handle the spin-3/2-structure of the Δ -resonance in a simple way⁶. Furthermore, for the investigated range in excitation energies we can safely use the no-sea approximation for the baryons. Thus we neglect processes involving anti-baryons and set the baryon spectral functions to zero for negative energies.

The following non-relativistic form of the interaction Lagrangian

$$\mathcal{L}_{N\Delta\pi}^{\text{int}} = -g_{\pi NN}\Psi_N^\dagger (\boldsymbol{\sigma}^\dagger \boldsymbol{\nabla}) (\boldsymbol{\tau}^\dagger \boldsymbol{\pi}) \Psi_N - g_{\pi N\Delta}\Psi_\Delta^\dagger (\boldsymbol{S}^\dagger \boldsymbol{\nabla}) (\boldsymbol{T}^\dagger \boldsymbol{\pi}) \Psi_N + h.c. \quad (5)$$

is used with the spinor-field operators Ψ_N and Ψ_Δ of the nucleon and Δ -resonance. Here $\boldsymbol{\sigma}$ and $\boldsymbol{\tau}$ denote the vectors of Pauli matrices in spin and isospin, respectively. Likewise, the vector \boldsymbol{S} defines the three spin-coupling matrices of spin 3/2 and 1/2 to spin 1, while \boldsymbol{T} is the same in isospin-space. In our scheme we neglect pion self-interactions ($\mathcal{L}_\pi^{\text{int}} \propto \pi^4$) which give rise to selfenergy diagrams of sunset type [38] as well as contributions from $\Delta\Delta^{-1}$ excitations. Both are of some importance at temperatures above 80 MeV, where they would even further broaden the pion spectral functions.

Furthermore we supplement an exponential formfactor

$$F(\mathbf{q}) = \exp(-\mathbf{q}^2/\Lambda^2) \quad (6)$$

at the πNN - and $\pi N\Delta$ -vertices. Values of $\Lambda = 440$ MeV and $g_{\pi N\Delta} = 0.02$ MeV⁻¹ are required for a decent fit of the pion-nucleon phase-shifts in the 33-channel⁷ and a proper vacuum spectral function of the Δ -resonance. For $g_{\pi NN}$ we use 0.007 MeV⁻¹ [46].

For the chosen Lagrangian mean-field terms drop out and the first diagrams for the Φ -functional in the baryon-pion sector which we use are:

$$\Phi_{N\Delta\pi} = \begin{array}{c} N \\ \circlearrowleft \\ \pi \\ \circlearrowright \\ N \end{array} + \begin{array}{c} \Delta \\ \circlearrowleft \\ \pi \\ \circlearrowright \\ N \end{array}$$

⁶ A fully relativistic formulation would require the use of special interactions as can be seen for example in ref. [44], which then would also have to be incorporated in the later introduced Migdal formalism.

⁷ This implies a cut-off dependence of the in-medium results. In models with a larger body of resonances, cf. [45], the cut-off Λ can be chosen above 700 MeV.

The lines represent the fully dressed propagators, while apart from the form-factor (6) the vertices remain bare.

Not all of the selfenergy terms obtained through (4) are of equal importance. For instance the Δ - π -loop contribution to the nucleon selfenergy is found negligible compared to the N - π -loop and thus neglected in the production runs. The retarded pion selfenergy can be obtained from a dispersion relation which in no-sea approximation does not require any renormalisation

$$\Pi^R(p) = \frac{i}{2\pi} \int dE' \frac{\Pi^{+-}(E', \mathbf{p}) - \Pi^{-+}(E', \mathbf{p})}{E' - E - i\epsilon}. \quad (7)$$

Interested in the pion modes a complete determination of the baryon selfenergies $\Sigma(p)$ is beyond the scope and not the aim of the present model. For simplicity we drop the real parts of $\Sigma(p)$, which would require a renormalisation procedure within a selfconsistent resummation scheme [47]. However the normalisation of the corresponding spectral functions is restored in each iteration step.

As is well known, the coupling of the pion to nucleon-hole (NN^{-1}) and ΔN^{-1} -states provides a strong softening of the pion modes already at normal nuclear densities. Since there are no indications from experiment for a pion condensate at normal nuclear density one has to include a repulsive force which shifts the spectral strength up to higher energies. This can be achieved by a repulsive short-range interaction between the baryons first introduced by Migdal [37]



For the Migdal parameters we used $g_{11} = 0.5$, $g_{22} = 0.6$ $g_{12} = 0.5$ without any form factor. At a momentum scale of 200 MeV/c for the relevant NN^{-1} excitations⁸ this choice is compatible with the recent parameter set of Suzuki [49] and Nakano [50] who calibrated it on Gamow-Teller transition strengths. These correlations are to be included in the retarded pion selfenergy in form of an RPA-resummation with particle-hole loops

$$\Pi_\pi^R = \text{---} \bigcirc \bigcirc \text{---} + \text{---} \bigcirc \bigcirc \bigcirc \text{---} + \dots,$$

where also mixtures with the Δ -resonance, i.e ΔN^{-1} -loops need to be considered. In the non-relativistic limit for the spinor structure of the baryons, only the spatial components of the Dirac matrices survive in all loops which,

⁸ These excitations, which essentially influence the ρ - ω mixing in matter, are mainly determined by g_{11} .

by symmetry arguments, are diagonal (for a fully relativistic treatment cf. [52]). Therefore, apart from a \mathbf{q}^2 -factor due to the difference between the pion-baryon coupling and the Migdal interaction the basic loops for the RPA-resummation are given by the normal pion selfenergy diagrams resulting from the Φ -functional (4)

$$\Pi_{\pi NN-1}^R = \text{---} \circlearrowleft \text{---} \quad \Pi_{\pi \Delta h}^R = \text{---} \circlearrowleft \circlearrowleft \text{---}$$

Thus, the RPA-resummation can be done without further problems. With the three possible vertices one finally obtains [45,11,12]

$$\Pi^R = (\mathbf{q}^2)^2 \frac{\Pi_{\pi NN-1}^R + \Pi_{\pi \Delta h}^R - (g_{11} - 2g_{12} + g_{22})\Pi_{\pi NN-1}^R \Pi_{\pi \Delta h}^R}{(\mathbf{q}^2 - g_{11}\Pi_{\pi NN-1}^R)(\mathbf{q}^2 - g_{22}\Pi_{\pi \Delta h}^R) - g_{12}^2 \Pi_{\pi NN-1}^R \Pi_{\pi \Delta h}^R} F(\mathbf{q}) \quad (8)$$

for the retarded pion selfenergy. The corresponding results together with those for the pion spectral function are shown in the Figs. 1 to 6.

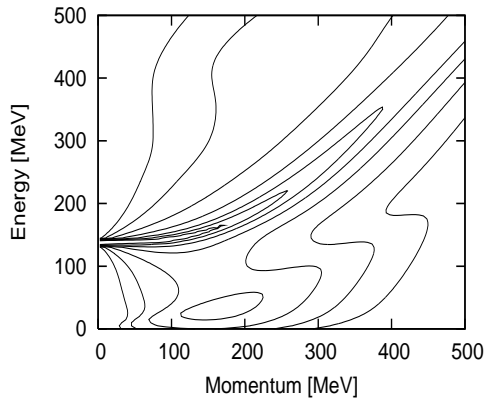


Fig. 1. Contour plot of the logarithm of the pion spectral function A_π at $T=0$ MeV and $\rho = \rho_0$. The line spacing covers half a decade.

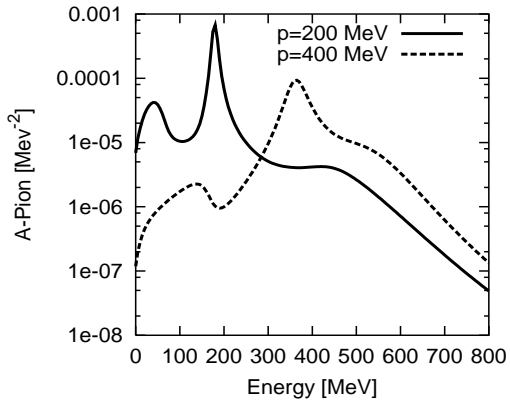


Fig. 2. Pion spectral function A_π at $T=0$ MeV and $\rho = \rho_0$ for two different momenta

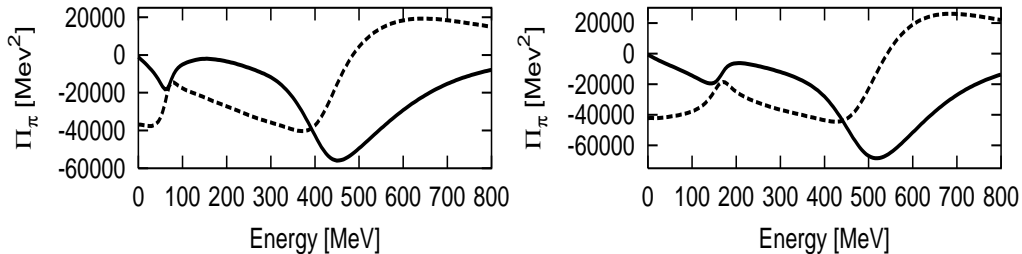


Fig. 3. Real (dotted line) and imaginary (full line) part of the pion selfenergy at $T=0$ MeV and $\rho = \rho_0$ for $|\mathbf{p}| = 200$ MeV (left panel) and $|\mathbf{p}| = 400$ MeV (right panel)

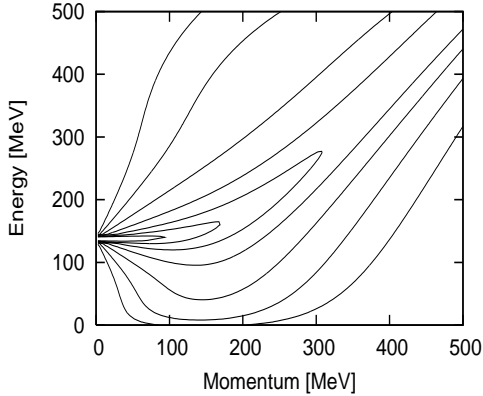


Fig. 4. Same as Fig. 1 for $T=120$ MeV

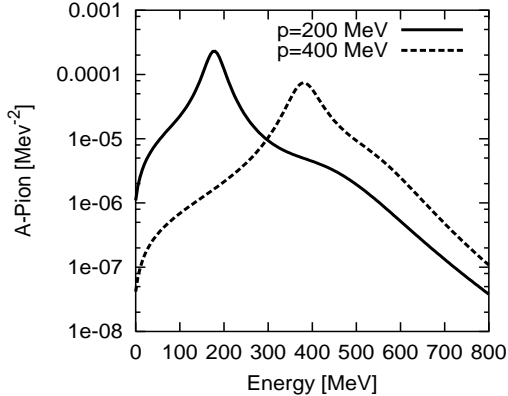


Fig. 5. Same as Fig. 2 at $T=120$ MeV

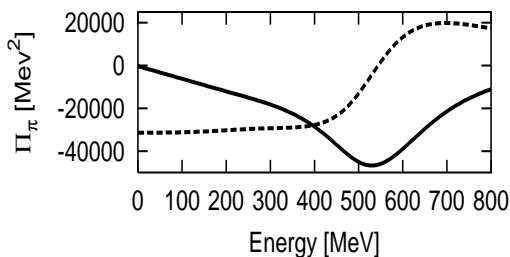
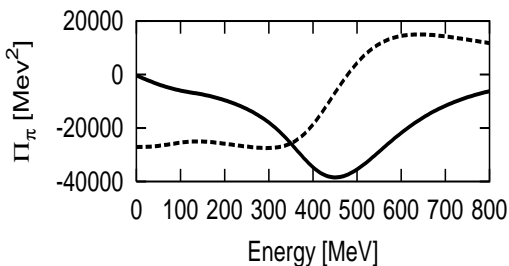


Fig. 6. Same as Fig. 3 at $T=120$ MeV

In the selfenergy and spectral function we see the effect of the coupling to the different baryonic excitations. The on-shell pole broadens and is shifted towards lower energies due to the net-attraction of the interaction in this kinematical region. This component strongly mixes with the ΔN^{-1} component which leads to the shoulders around this peak. This component appears in the time-like region for low momenta, while it traverses to the space-like region for higher momenta. At low energies an entirely space-like pion component appears due to NN^{-1} excitations. From the kinematics it is clear that this component stays in the space-like region for all momenta. Such space-like pion modes have to be interpreted as a scattering process on the baryons in the matter mediated by the exchange of pions. Due to this component, the pion spectral function has non-vanishing strength at all energies, such that in all processes where pions are involved all thresholds disappear. Due to the short-range Migdal repulsion there is no spectral component where the peak position decreases towards lower energies when one increases the momentum. The form of the spectral function turns out to be very sensitive on values for the Migdal parameters and the formfactor F . In addition, in the literature one finds quite different procedures to incorporate the formfactor in the Migdal resummation. Some of them include formfactors also for the Migdal-vertices [48–50]⁹. We

⁹ Following the Korpa-Malfliet [48,51] prescription for the Migdal vertices we could qualitatively reproduce their results as a check for our numerics.

followed the approach from refs. [11–13] with formfactor-free Migdal vertices. The difference between these two techniques turns out to have a great effect on the shape of the pion spectral function for momenta in the order of 400 MeV. For higher temperatures all structures are smoothed out and the value of the selfenergy even decreases because of limited number of available nucleons to scatter.

3.2 Pions and Vector-mesons

In this chapter we study the influence of the medium-modified pion-modes on the spectral functions of the ρ - and ω -mesons. The vacuum widths of these resonances are generated through the decay into two pions in the case of the ρ -meson, respectively three pions for the ω -meson. For the ω -meson we choose the indirect decay via the ρ -meson (the so called Gell-Mann, Sharp and Wagner (GSW) process [54]) because, as shown by Theileis [53], this is the dominant contribution in vacuum. The interaction Lagrangian defining the vertices is given by [55–57]

$$\mathcal{L}_{\pi\rho\omega}^{\text{int}} = g_{\rho\pi\pi}\rho^\mu(\pi\overleftrightarrow{\partial}_\mu\pi) + g_{\omega\rho\pi}\epsilon^{\alpha\beta\mu\nu}\omega_\alpha\partial_\beta\rho_\mu\partial_\nu\pi, \quad (9)$$

for a review see [58]. In this sector we are lead to the following Φ -functional approximation

$$\Phi = \begin{array}{c} \pi \\ \text{---} \\ \text{---} \\ \text{---} \\ \rho \\ \text{---} \\ \text{---} \\ \pi \end{array} + \begin{array}{c} \rho \\ \text{---} \\ \text{---} \\ \text{---} \\ \omega \\ \text{---} \\ \text{---} \\ \pi \end{array} \quad (10)$$

The coupling vertices of both terms are adjusted to the $\pi\pi$ -scattering phase shifts together with the electromagnetic formfactor of the pion and to the vacuum decay width of the ω -meson, respectively. From the point of view of a Φ -derivable approximation we neglected the coupling of the ρ - ω -loop back to the pion. This process is expected to contribute only marginally to the low energy region of the pion spectrum, which turns out to be the most relevant part to determine the in-medium damping width of the ω -meson. Therefore only the following retarded selfenergies are included:

$$\Pi_{\mu\nu}^R{}_{\rho\pi\pi} = \begin{array}{c} \pi \\ \text{---} \\ \text{---} \\ \text{---} \\ \pi \end{array} \quad (11)$$

$$\Pi_{\mu\nu\ \omega\rho\pi}^R = \text{Diagram} \quad (12)$$

The correlation between ρ - and ω -meson modes results from the ω -meson selfenergy (12) and the reverse process encoded in the coupling of the ρ -meson to the ω - π -loop

$$\Pi_{\mu\nu\ \rho\omega\pi}^R = \text{Diagram} \quad (13)$$

which both are included selfconsistently. Since the model omits higher lying degrees of freedom the in-medium changes of the real parts of the vector-meson selfenergies are less precisely determined within the model space. Therefore we drop them during the selfconsistent iterations, while restoring the normalisation of the spectral functions at each step. A posteriori, we checked for the thus ignored real parts of the loops using a counter-term scheme which through vector dominance fixes the photon mass (i.e. at $q^2 = 0$) to be zero with residue equal one in vacuum. It gave values of $\text{Re } \Pi/(2p^0)$ which are by far less than the corresponding widths of the vector mesons and therefore negligible. Keeping this subtraction scheme also at finite T , i.e. ignoring contributions from hidden divergences [47] and tadpoles, which solely lead to an additional T -dependent mass shift, we still obtained insignificant changes in this quantity. In a later section we supplement a discussion on the sensitivity of the results on possible changes of the vector-meson masses in matter.

3.3 *Transversality of the vector-meson polarisation tensors*

The resulting polarisation-tensors (11 - 13) have to be four-transversal because of current conservation. In normal perturbation theory this is guaranteed order by order. In the Dyson approach, where one sums up a restricted subclass of diagrams to infinite order, one generally violates Ward identities on the correlator level. Thus the polarisation tensor may contain four-longitudinal components $\Pi_i^{\mu\nu}(q)$, which have to be absent and which may lead to the propagation of unphysical degrees of freedom. From general grounds, this deficiency can be cured by corresponding vertex corrections. Without further approximations, however, this leads to a presently intractable scheme of Bethe-Salpeter equations which accounts for the required t -channel exchanges required by crossing symmetry. We circumvent this problem in the following way. From transport considerations [59] it is known that such polarisation tensors have at

least two relaxation times. Because of charge conservation, one of these times has to be infinite, implying that the component $\Pi^{00}(q)$ vanishes exactly for $\mathbf{q} = 0$ and $q_0 \neq 0$, while the second relaxation time is clearly finite. Such a result can never be reached in a truncated Dyson-resummation scheme where all relaxation times are finite, because they are determined by the damping-time scale of the dressed propagators involved in the loops. On the other hand, the spatial components of the polarisation tensor, given by the autocorrelation of spatial currents, have solely finite and short correlation times which can be expected to be safely approximated within a Dyson resummation scheme. Therefore our strategy assumes the spatial components of the polarisation tensors $\Pi_{\mu\nu}^R$ to be given by the selfconsistent loops, while the time-components are to be corrected such that the full tensor becomes four-transversal. This is achieved by using a projection technique where the full tensors (11 - 13) are decomposed into a four-longitudinal part Π_l and two four-transversal parts Π_L and Π_T which are three-longitudinal and three-transversal, respectively,

$$\begin{aligned}
\Pi^{\mu\nu}(q) &= \Pi_l^{\mu\nu}(q) + \Pi_L^{\mu\nu}(q) + \Pi_T^{\mu\nu}(q) \\
\Pi_L^{\mu\nu}(q) &= \left(-g^{\mu\nu} - \delta^{\mu\nu} + \frac{q^\mu q^\nu}{q^2} + \frac{\mathbf{q}^\mu \mathbf{q}^\nu}{\mathbf{q}^2} \right) \cdot \Pi_L(q) \\
\Pi_T^{\mu\nu}(q) &= \left(\delta^{\mu\nu} - \frac{\mathbf{q}^\mu \mathbf{q}^\nu}{\mathbf{q}^2} \right) \cdot \Pi_T(q).
\end{aligned} \tag{14}$$

Here $g^{\mu\nu}$ is the metric tensor, whereas $\delta^{\mu\nu}$ and \mathbf{q}^μ have vanishing time components. We do not specify the Π_l part any further, since this part has just to be dropped due to current conservation. The scalar functions Π_L and Π_T can be calculated solely from the spatial parts of the polarisation tensors using the following traces

$$\begin{aligned}
\Pi_1 &= \frac{q^i q^k}{\mathbf{q}^2} \Pi^{ik} = \frac{(q^0)^2}{q^2} \cdot \Pi_L \\
3\Pi_3 &= \text{Tr}_3 [\Pi^{ik}] = -g_{ik} \Pi^{ik} = 2\Pi_T + \frac{(q^0)^2}{q^2} \cdot \Pi_L \quad \text{or} \\
\Pi_L &= \frac{q^2}{(q^0)^2} \cdot \Pi_1; \quad \Pi_T = \frac{1}{2} (3\Pi_3 - \Pi_1).
\end{aligned} \tag{15}$$

Due to the traces, the complicated Lorentz-structure of the interaction vertices (9) in the loops can be reduced entirely to expressions involving the four-, respectively, three-vector squares q^2 , p^2 , p'^2 and \mathbf{q}^2 , etc. of the external and internal momenta involved in the loops. Furthermore, three-longitudinal and transverse modes decouple such that the corresponding spectral functions $A_L(q)$ and $A_T(q)$ are directly given by the scalar functions $\Pi_L(q)$ and $\Pi_T(q)$ of the corresponding components of the polarisation tensors.

3.4 Vector-meson spectral functions in matter

With the dressed pion spectral function from section 3.1, the three-longitudinal respectively three-transversal polarisation tensors and spectral function of both vector-mesons can now be calculated. In Figs. 7 to 14 we show the results for normal nuclear density at different temperatures¹⁰

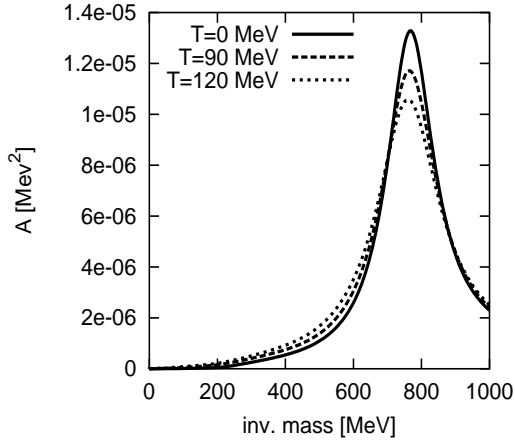


Fig. 7. 3-longitudinal ρ -meson spectral function $A_{\rho,L}$ at $p=200$ MeV and $\rho = \rho_0$ for different temperatures

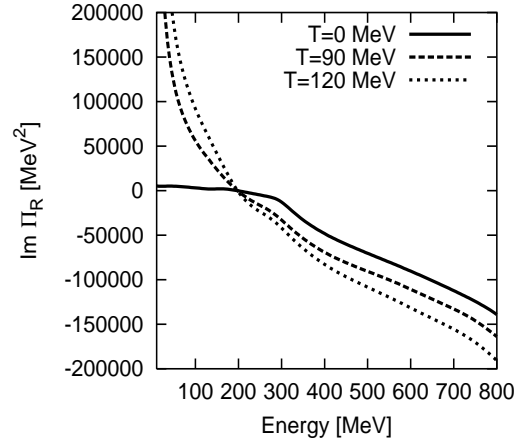


Fig. 8. 3-longitudinal part of the ρ -meson selfenergy $\text{Im}\Pi_{\rho,L}^R$ at $p=200$ MeV and $\rho = \rho_0$ for different temperatures

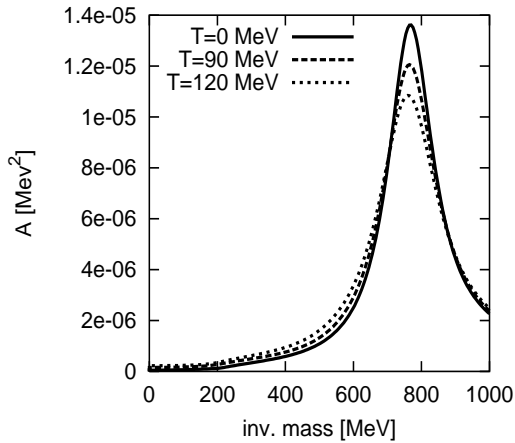


Fig. 9. 3-transversal ρ -meson spectral function $A_{\rho,T}$ at $p=200$ MeV and $\rho = \rho_0$ for different temperatures

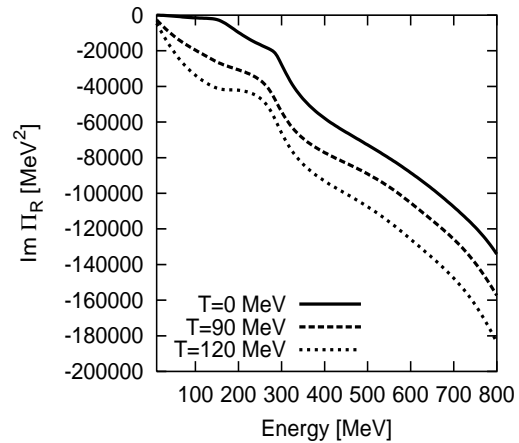


Fig. 10. 3-transversal part of the ρ -meson selfenergy $\text{Im}\Pi_{\rho,T}^R$ at $p=200$ MeV and $\rho = \rho_0$ for different temperatures

¹⁰Please note that by definition, cf. (14), $\text{Im}\Pi_L^R$ vanishes on the light cone $p^2 = 0$ and becomes positive in the space-like region.

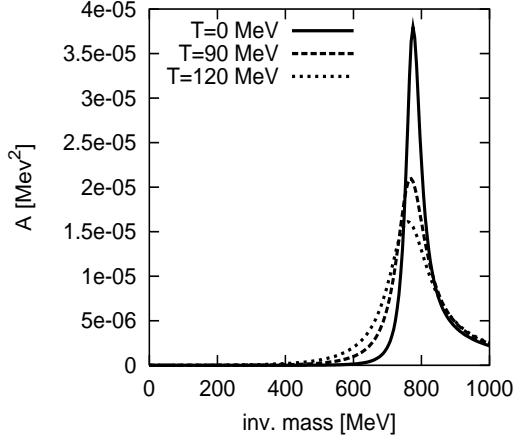


Fig. 11. $A_{\omega,L}$ at $p=200$ and $\rho = \rho_0$

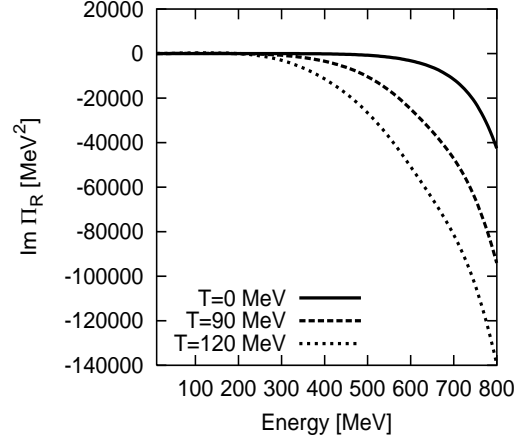


Fig. 12. $\text{Im}\Pi_{\omega,L}^R$ at $p=200$ MeV and $\rho = \rho_0$

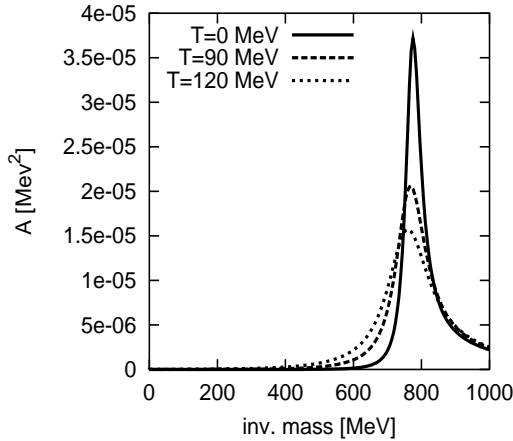


Fig. 13. $A_{\omega,T}$ at $p=200$ MeV and $\rho = \rho_0$

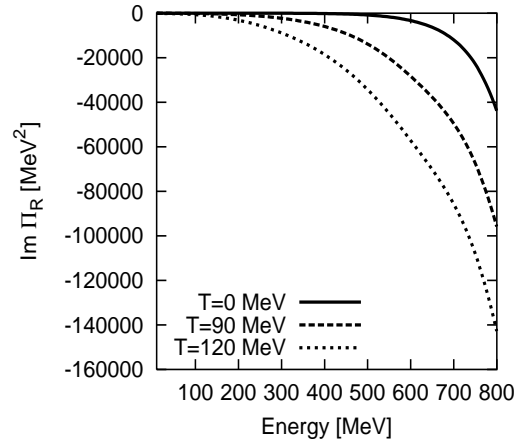


Fig. 14. $\text{Im}\Pi_{\omega,T}^R$ at $p=200$ MeV and $\rho = \rho_0$

The main effect towards finite densities and/or finite temperatures is the disappearance of thresholds present in the free particle kinematics for the pions in the loops. The spectral strength starts right at zero energy for both vector-mesons, though less visible for the ω -meson due to the smallness of the coupling. This has significant consequences for the low mass region of the corresponding dilepton yields (cf. next section). The temperature has no great influence on the ρ -meson spectrum, while the ω -meson width increases significantly. For the latter effect indirectly the nucleon–nucleon-hole excitations are of special importance as discussed later.

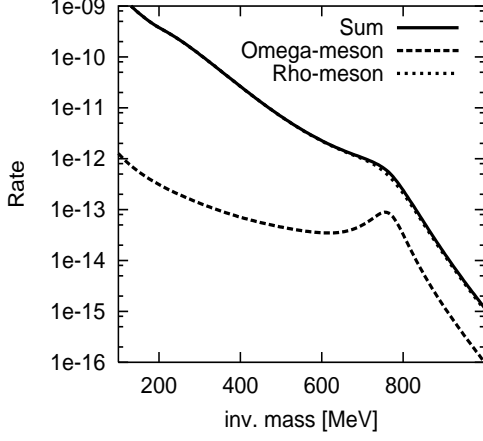


Fig. 15. e^+e^- -rate at $T=60$ MeV $\rho = \rho_0$

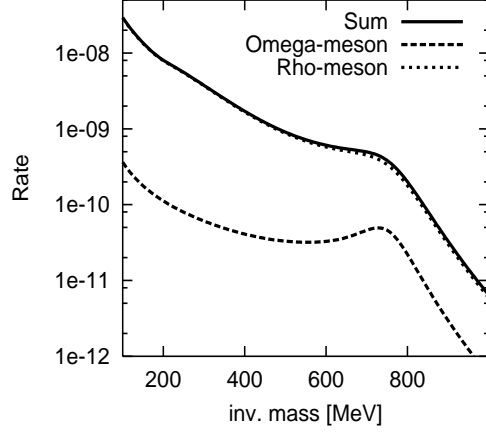


Fig. 16. e^+e^- -rate at $T=120$ MeV $\rho = \rho_0$

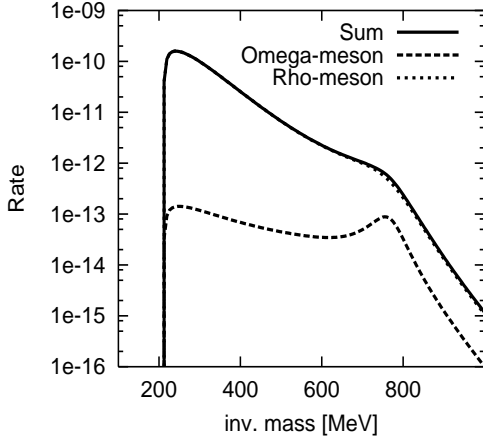


Fig. 17. $\mu^+\mu^-$ -rate at $T=60$ MeV $\rho = \rho_0$

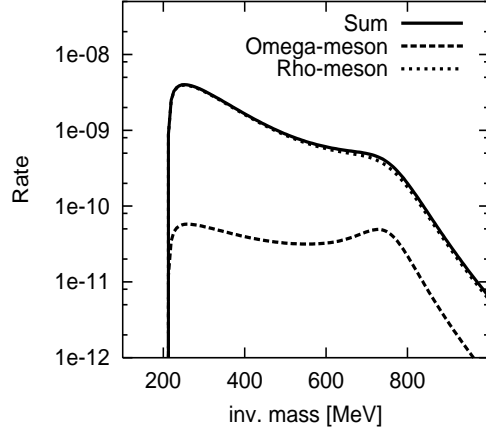


Fig. 18. $\mu^+\mu^-$ -rate at $T=120$ MeV $\rho = \rho_0$

3.5 Dileptons

Using vector-dominance we can calculate [60,61] the production-rate for dilepton pairs (e^+e^- and $\mu^+\mu^-$)

$$\frac{dR}{d^4q d^3x dt} = \frac{\alpha^2}{6\pi^3 q^2} \sqrt{\frac{q^2 - 4m_l^2}{q^2}} \left(1 + \frac{2m_l^2}{q^2}\right) \times \sum_{\nu} \frac{m_{\nu}^4}{g_{\nu\pi\pi}^2 (1 - 4\pi\alpha g_{\nu\pi\pi}^2)} [2A_{\nu,T}(q, T) + A_{\nu,L}(q, T)] n_B(q, T) \quad (16)$$

from the in-medium spectral functions of the ρ - and ω -meson. Here $n_B(q_0, T)$ is the thermal Bose-Einstein weight, while m_{ν} and $g_{\nu\pi\pi}$ denote the vector-meson mass and the coupling constant of the meson to two pions. The mass of

the lepton, electron or muon, is symbolised by m_l . In our model we obtain the results displayed in Figs. 15 to 18 for the direct decay of a vector-resonance into a dilepton pair via an intermediate time-like photon.

With applications to nuclear collisions in mind, we use the vacuum expressions for the photon- and lepton-propagators, since these particles interact only weakly, such that they do not get modified by the surrounding medium. In addition, we used the coupling constants from [58] in order to describe the partial decay width of both mesons into dileptons. One can see that, due to the thermal weight and the broad spectral functions, the dilepton spectra are essentially falling over the whole energy range. This would clearly be different if the vacuum spectral function for the ω -meson had been used here. The $\mu^+\mu^-$ -spectrum has a threshold at twice the muon mass. At higher invariant mass both di-lepton spectra merge, because then the muon mass becomes negligible in comparison with the energy. The contributions of the ω -meson are hardly visible in the total spectra because of its increased width. For equal widths of both mesons the contributions of the ω -meson falls below that of the ρ -meson by one order of magnitude because of the smaller partial decay width into dileptons.

In the following we explicitly analyse the influence of the various components of the pion spectral function on the vector-mesons and thus on the dilepton spectra. Formally we do this by splitting the spectral function of the vector-meson into the various components related to the different processes feeding into this vector-meson channel. Thus, decomposing the total damping width into partial widths $\Gamma_{v,\text{tot}}(p) = \sum_i \Gamma_{v,i}(p)$ the dilepton yield can be brought into a Breit-Wigner like form with partial in- and out-widths

$$\begin{aligned} \frac{dR}{d^4q d^3x dt} &= \frac{3}{(2\pi)^4} n_T(q_0) \sum_v A_v(q) (-2\text{Im} \Pi_{v,e^+e^-}) \\ &= \frac{3}{(2\pi)^4} n_T(q_0) \sum_{v,i} \frac{4 q_0^2 \Gamma_{v,i} \Gamma_{v,e^+e^-}}{(q^2 - m_v^2)^2 + q_0^2 \Gamma_{v,\text{tot}}^2} \end{aligned} \quad (17)$$

(suppressing the tensor structure of spectral function and polarisation tensor which leads to a degeneracy factor 3 for vector particles). Here, Γ_{v,e^+e^-} is the dilepton decay width of vector-meson v .

We start the discussion of the effects on the ω -meson. In the medium there are three major processes contributing to its damping width, illustrated by perturbative “time-flow” diagrams where the time is running from left to right and vertical lines denote a virtual space-like propagator, which mediates a two-body interaction:

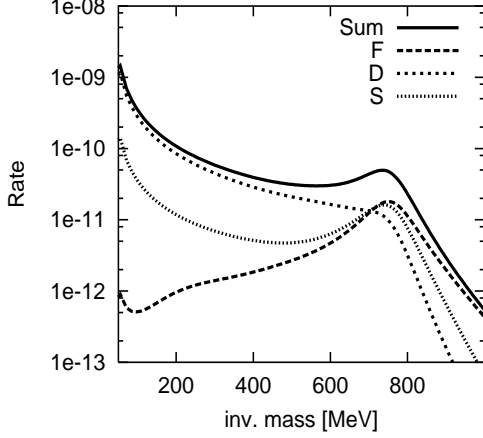


Fig. 19. e^+e^- -rate from the decay of the ω -meson at $T=120$ MeV $\rho = \rho_0$ divided into different contributions:

- F: $\pi\rho \rightarrow \omega$
D: $\rho \rightarrow \pi\omega$
S: $\rho N \rightarrow \omega N$

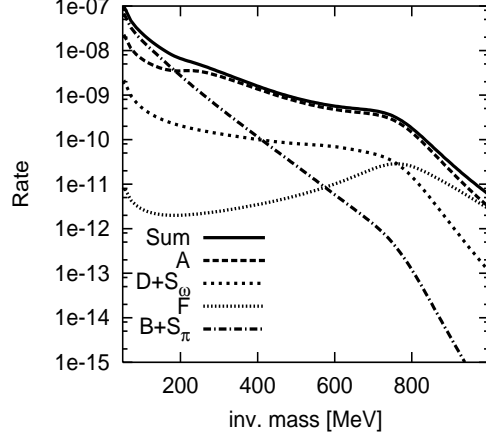
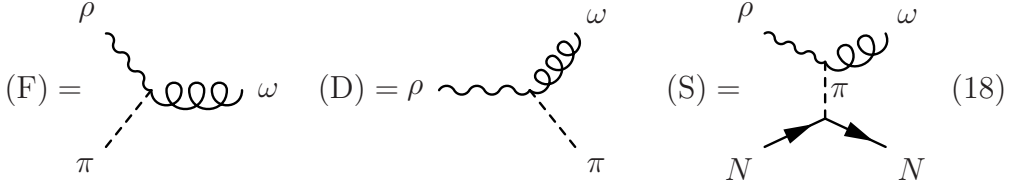


Fig. 20. e^+e^- -rate from the decay of the ρ -meson at $T=120$ MeV $\rho = \rho_0$ divided into different contributions:

- A: $\pi\pi \rightarrow \rho$ F: $\pi\omega \rightarrow \rho$
B: $\pi \rightarrow \pi\rho$ D: $\omega \rightarrow \pi\rho$
 S_π : $\pi N \rightarrow \rho N$ S_ω : $\omega N \rightarrow \rho N$



Here the subsequent decay of the ω -meson into the virtual time-like photon and its final decay into the lepton pair is not illustrated. In the selfconsistent calculation all these processes are included automatically by using dressed propagators. For the first process (F), $\rho\pi \rightarrow \omega \rightarrow e^+e^-$, the ω -meson is formed by the fusion of a ρ -meson with a quasi-real, in-medium pion. Its inverse exists already in vacuum and determines the vacuum decay width of the ω -meson. The second process (D), $\rho \rightarrow \pi\omega \rightarrow \pi e^+e^-$, corresponds to a ρ -Dalitz-decay via an intermediate ω -meson. In the selfconsistent calculations, both above mentioned processes just differ in the sign of the pion energy in the $\pi\rho$ -loop of the ω -selfenergy (12). The process (S) in (18) corresponds to the scattering $\rho N \rightarrow \omega N$ mediated by a virtual, i.e. space-like pion exchange. In view of the pion modes at zero temperature (cf. Fig. 1) we isolate this space-like component by a cut on the far space-like region with pion loop momenta with $|\mathbf{p}| > 2|p^0|$ in (12). At $T = 120$ MeV this separation is by far less evident in view of the broad structure of the pion spectral function (Fig. 4). Thus the different components of the processes displayed in Fig. 19 somewhat depend on this cut. In addition to the fusion width (F), which constitutes just a temperature dependent modification of the vacuum width (e.g. accounted for by Schneider and Weise [32]) a genuine in-medium process, namely the scattering process (S), contributes with comparable strength at the nominal

resonance position. The “Daliz”-decay of the ρ -meson (D) dominates the low mass region.

In summary of this analysis: a major portion to the ω spectrum results from processes (S) which are not accounted for in the simple on-shell treatment. These contributions, however, sensitively depend on the in-medium properties of the virtual pion cloud, which certainly needs further clarifying investigations before quantitative conclusions can be drawn.

The same type of processes as in (18) also occur for the ρ -meson just interchanging ρ with ω , listed in the ρ -meson decomposition given in Fig. 20 as (F), (D) and (S_ω). However, these ω -induced components are less important compared to the coupling to the two-pion channels

$$(A) = \begin{array}{c} \pi \\ \text{---} \\ \diagdown \\ \text{---} \\ \pi \end{array} \begin{array}{c} \text{---} \\ \diagup \\ \text{---} \\ \rho \end{array} \quad (B) = \pi \text{---} \begin{array}{c} \text{---} \\ \diagup \\ \text{---} \\ \rho \end{array} \begin{array}{c} \text{---} \\ \diagdown \\ \text{---} \\ \pi \end{array} \quad (S_\pi) = \begin{array}{c} \pi \\ \text{---} \\ \diagdown \\ \text{---} \\ \rho \end{array} \begin{array}{c} \text{---} \\ \diagup \\ \text{---} \\ \pi \end{array} \begin{array}{c} \text{---} \\ \diagdown \\ \text{---} \\ N \end{array} \begin{array}{c} \text{---} \\ \diagup \\ \text{---} \\ N \end{array} \quad (19)$$

At invariant masses above 300 MeV, the $\pi^+\pi^-$ -annihilation process (A) is clearly dominant. Processes (B) and (S_π) are not present in any on-shell treatment of the pion as they solely arise from genuine off-shell components of the pion spectral function. In this respect (B) can be interpreted as a bremsstrahlung process radiated off a pion scattered in the medium, while process (S) corresponds to inelastic $\pi N \rightarrow \rho N$ scatterings mediated via virtual pion exchange. The latter two components, which emerge completely consistently within the model, only contribute to the very low-mass part of the invariant mass spectrum.

3.6 Dependence on density and temperature

We restrict the discussion of the dependence of the vector-meson properties on density and temperature to the case where the baryons and the vector-mesons retain their vacuum masses and use a cut-off $\Lambda = 440$ MeV (6) at the pion-nucleon- and pion-nucleon- Δ -vertices (5). The results for the damping width at resonance condition, i.e. at the vacuum masses, are summarised in Figs. 21 to 24.

Both vector-mesons show a strong non-linear dependence on the baryon density ρ induced by the selfconsistent treatment. For the ρ -meson the relative changes are less dramatic due to the large vacuum width of 150 MeV from the $\pi\pi$ -annihilation channel. The temperature effects are different. Here, with increasing temperature, the ρ -meson width stays nearly constant at nuclear

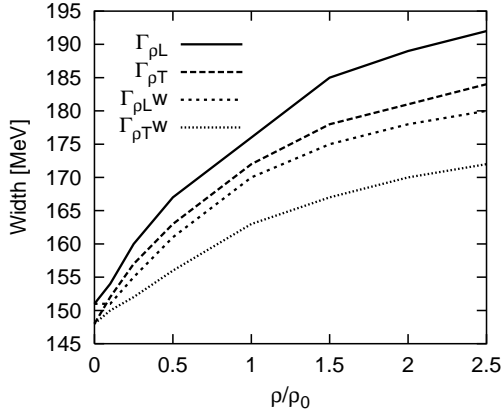


Fig. 21. Γ_ρ at $T=30$ MeV depending on the density. Γ_w marks the process with only $\rho \rightarrow \pi\pi$.

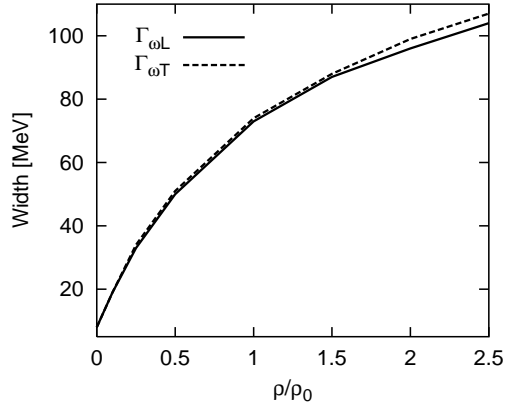


Fig. 22. Γ_ω at $T=30$ MeV depending on the density.

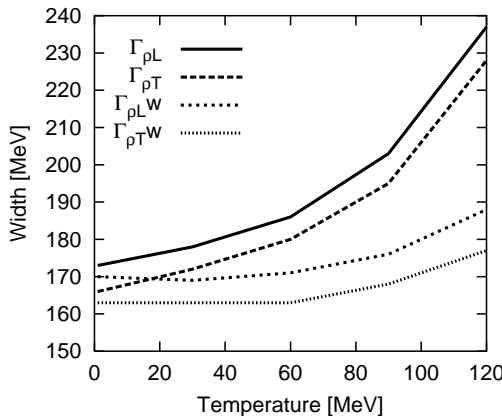


Fig. 23. Γ_ρ depending on the temperature. Γ_w marks the process with only $\rho \rightarrow \pi\pi$.

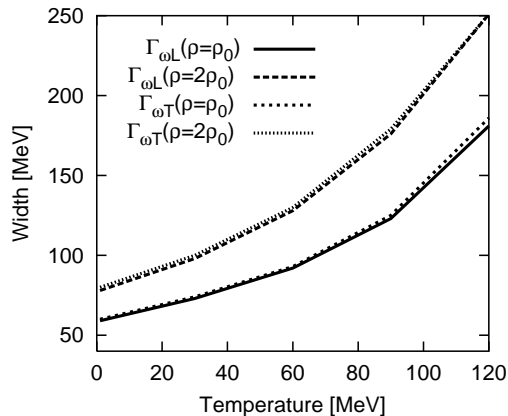


Fig. 24. Γ_ω depending on the temperature.

saturation density ρ_0 . The main contribution to the increase of the total width comes from the processes $\rho \rightarrow \omega\pi$ and $\rho\pi \rightarrow \omega$. On the other hand the ω -meson is seen to have a strong dependence on temperature inducing a width change of up to a factor of 3 in the temperature range from $T=0$ MeV to $T=120$ MeV. For both mesons the temperature effects are due to an enhanced scattering with the pions in the medium¹¹. In comparison to the perturbative calculations by Schneider and Weise [32] the selfconsistent treatment produces an even broader ω spectral function, due to the appearance of the low energy, space-like, pion modes. The QCD sum rules approach of Klingl and Weise [63] and also the low-density expansion scheme of Lutz et.al. [17] produced ω -meson widths of about 40 MeV at $T = 0$ and $\rho = \rho_0$, which is nearly 2/3 of ours. The slight deviations to our results can be understood by the change of the vector-meson masses in medium in their models as discussed in chapter

¹¹This has already been pointed out by Roy et al. [24] who also indicated that the process $\omega \rightarrow \rho\pi$ might be increased in-matter due to mass shifts.

3.7. Compared to the σ - ω -mixing model of Saito et al. [33] we cannot account for level-level repulsion in our model, as we do not include the real parts of the vector-meson selfenergies.

Altogether the ω -meson width sensitively depends on the properties on the in-medium pion cloud. An increase of the cut-off scale Λ of the πNN -formfactor (6) for instance would significantly enhance the RPA pion-modes and induce a further increase of the ω -meson width. Once the ω -meson width increases beyond 50 MeV, it loses its prominent peak-structure and its component can no longer be easily resolved in the dilepton spectrum due to the dominance of the ρ contribution.

3.7 Dependence on the vector-meson masses

Our description of the vector-meson sector is not as complete as to permit definite predictions for the mass shifts of the vector-mesons, i.e. the real parts of the vector-meson selfenergies. This is a subject of current debate and investigations and requires a more complete model space within hadronic descriptions [8,17] or support from QCD, e.g. in form of sum-rule constraints [25–29]. For simplicity the real parts of the vector-meson selfenergies are put to zero in the results presented above. On the other hand we can explore the effect of mass shifts by simply changing the masses by hand. For the following discussion we concentrate on the damping widths (longitudinal and transverse) of the vector-mesons at the in-medium mass position $q^2 = m_v^2$ for a typical momentum of 200 MeV/c given by

$$\Gamma_{v,L/T} = -\text{Im} \Pi_{v,L/T}^R(q)/q_0 \Big|_{q^2=m_v^2}. \quad (20)$$

A phenomenological lowering of the ρ -meson mass, e.g. within the Brown-Rho scaling scheme [15], has been considered by many authors. This leads to an enhanced strength in the mass region below the ρ -meson vacuum mass. From the calculations thus far the mass dependence of the vector-meson damping widths at $T = 0$ and saturation density can approximately be read off by i.e. inspecting Figs. 10 and 14. They predict marginal changes for the ρ -meson width. Thus, the entire ρ -meson strength will be shifted, e.g. towards lower masses, with the extra benefit that the thermal weight factor in (17) enhances the dilepton yield by about a factor $\exp(\Delta m_\rho/T)$. The ω -meson shows sensitive changes of its damping width as a function of its invariant mass. Since the only channel, to which the ω -meson couples to in our model, is the π - ρ -channel, we expect Γ_ω to depend sensitively only on the mass difference or ratio between the ρ - and ω -meson masses.

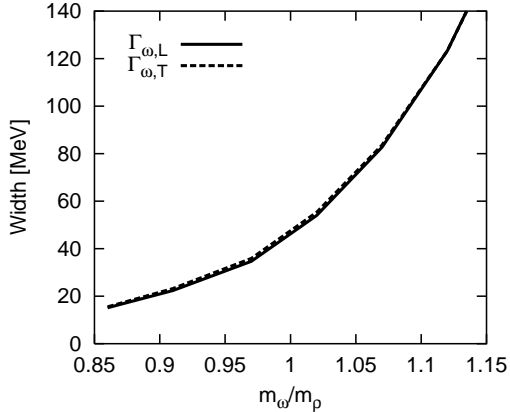


Fig. 25. Γ_ω at $T=0$ MeV and $\rho = \rho_0$ depending on the mass ratio m_ω/m_ρ .

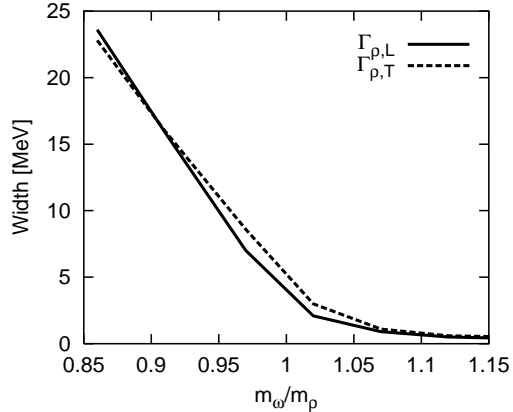


Fig. 26. Partial decay width $\Gamma_{\rho \rightarrow \omega\pi}$ for the process $\rho \rightarrow \omega\pi$ at $T=0$ MeV and $\rho = \rho_0$ depending on the mass ratio m_ω/m_ρ .

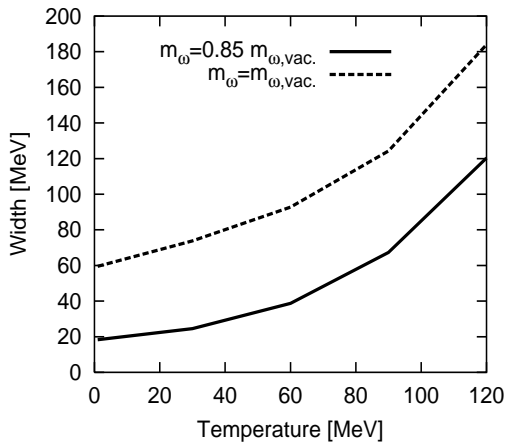


Fig. 27. Width of the ω -meson with and without reduced mass for normal nuclear density and different temperatures.

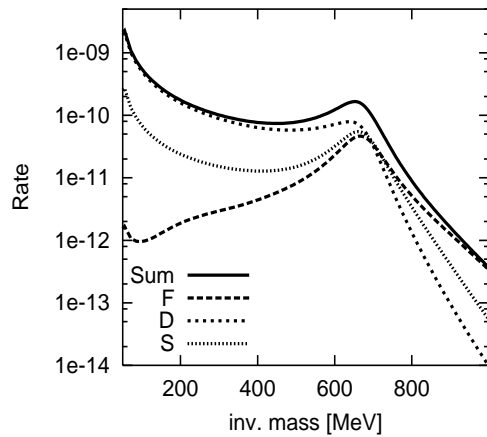


Fig. 28. e^+e^- -spectra resulting from the decay of the ω -meson at $m_\omega = 0.85m_{\omega,vac.}$, $T=120$ MeV and $\rho = \rho_0$, For notations see Fig. 19.

The explicit results for the dependence on m_ω/m_ρ for $T = 0$ and normal nuclear density can be found in the Figs. 25 and 26 for the ω -meson and for the partial width $\Gamma_{\rho \rightarrow \omega\pi}$ of the ρ -meson, respectively. Due to the dominance of the $\pi\pi$ -annihilation channel, the latter has minor impact on the total ρ -meson width. The displayed dependence follows expectations from phase-space arguments. Our results compare favourably with the calculations of Klingl and Weise [63] and Lutz et.al. [17], who used QCD sum rules or the low density theorem for the determination of the mass shifts. Although in the Klingl and Weise result [63] the mass of the ω -meson is lowered by 15% relative to the ρ -meson mass, which would infer a much smaller width, one has to take into account that in those calculations a much broader ρ -meson ($\Gamma_\rho \approx 300$ MeV) was used inducing a compensating increase of the ω -width. We also studied the vector-meson mass dependence at finite temperature. In Fig. 27 we compare

the width of the ω -meson with a mass reduced by 15% to the width without such a reduction¹². We find that the overall offset is nearly the same for all temperatures. According to this, the relative effect decreases for higher temperatures. This can be understood because kinematical effects, like mass shifts, are of less importance for broad spectral functions. In Fig. 28, we show the effect of this mass shift on the dilepton spectra. We observe that the peak structure becomes more prominent because of the smaller width of the ω -meson and that the total rate is enhanced. This enhancement is due to the thermal weight which increases exponentially towards lower temperature.

4 Conclusions

We have investigated the in-medium effects on the light vector-mesons due to the modification of the pion modes in nuclear matter at finite density and temperature. To isolate this effect only the coupling of the vector-mesons to the pion modes has been considered so far. The direct coupling to baryonic currents along the lines of refs. [8,9,17] within a selfconsistent scheme will be the subject of a forthcoming study.

Within a selfconsistent Dyson resummation scheme, the nucleon and $\Delta(1232)$ -resonance were included as the main degrees of freedom in the baryon sector. Besides the direct πNN and $\pi N\Delta$ couplings, accounted for in selfconsistent selfenergies up to one-loop order, also the short-range RPA correlations of Migdal type [37] were included in order to get a realistic behaviour of the low energy pion modes. While for the meson-baryon couplings a non-relativistic approximation was employed, the kinematics of all particles was treated relativistically. The so obtained in-medium spectral functions of the pion provide the source for the vector-meson selfenergies through the $\pi\pi\rho$ and $\pi\rho\omega$ coupling vertices. While the former already induces the strong damping width of the ρ -meson in vacuum, the latter becomes essential for the strong vector-meson “mixing” at finite densities and temperatures. Consequences for the resulting in-matter dilepton spectra from the electromagnetic decay of the vector-mesons have been discussed.

The polarisation-tensor for the vector-mesons has to be four-transversal such that no unphysical degrees of freedom are propagated. This was achieved by a projector technique (see Eq. (14) ff.) which provides the three-longitudinal and three-transversal parts, respectively. These two parts are identical in the vacuum due to Lorentz invariance, while they may differ in the medium.

As an important result of our investigations we find a strong mixing of both

¹²We show the mean value of longitudinal and transverse widths Γ_L and Γ_T .

vector-meson modes in-matter. It is induced by the low-lying space-like pion modes which essentially arise from the coupling to particle-hole excitations. As a consequence, the ω -meson damping width drastically broadens both, with increasing baryon density and temperature reaching values of 100 MeV or even above.

The quantitative results on the in-medium properties of the vector mesons still depend on the model assumptions and parameters for the in-medium pion physics such as the Migdal parameters and the formfactors for the πNN and $\pi N\Delta$ vertices. Despite more than two decades of work in this field, the in-medium properties of the pion are not yet conclusively settled. Thus, further improvements, especially concerning the NN^{-1} -component, are required for a quantitative understanding of the in-medium broadening of the light vector-meson spectral functions, especially of the ω -meson. Here other techniques like the recent calculations from Lutz and Korpa [62] are to be mentioned which may offer alternative and quantitative strategies to understand the spectral function of the pion and thus provide a reliable basis for the calculations of the vector-mesons properties. As our approach qualitatively incorporates most of the relevant contributions to the pion spectral function, all qualitative features should already be visible in our results. Even if the situation at zero temperature and saturation density may eventually become quantitatively settled, the extrapolation of the effective interactions to finite temperatures may require further adaptations.

The broad ω -meson distributions, as found in our calculations, will make it difficult to isolate this in-medium component in dilepton spectra. It will be detected in competition with the much stronger electromagnetic decay rates of the ρ -meson. Therefore complementary experiments which directly isolate the ω -component e.g. partly through hadronic channels, such as in the recent TAPS-experiments [6,7], are vital to clarify the situation. In nuclear collision experiments, one further has to face the fact that contributions from final-state interaction always arise. Such asymptotic state vector-mesons show the signature of the corresponding vacuum spectral functions and thus may hide the here addressed in-matter components.

Acknowledgement

The authors acknowledge fruitful discussions with C. Greiner, B. Friman, C.L. Korpa, S. Leupold, M.F.M. Lutz, D. Voskresensky and J. Wambach at various stages of this work.

References

- [1] J. Friese et al., *Nuc. Phys.* A654 (1999) 1017c
- [2] H.S. Matis, *Nuc. Phys.* A583 (1995) 617c
- [3] J.P. Wessels et al., *Nuc. Phys.* A715 (2003) 262c
- [4] A.L.S. Angelis et al., *Eur. Phys. J.* C13 (2000) 433
- [5] K. Ozawa et al., *Phys. Rev. Lett.* 86 (2001) 5019
- [6] J.G. Messchendorp et al., *Eur. Phys. J.* A11 (2001) 95
- [7] V. Metag, *Prog. in Part. Phys.* 50 (2003) 635
- [8] W. Peters et al., *Nucl. Phys.* A632 (1998) 109
- [9] M. Post, S. Leupold and U. Mosel, *Nuc. Phys.* A689 (2001) 753
- [10] R. Rapp and J. Wambach, *Adv. Nuc. Phys.* 25 (2000) 1
- [11] M. Urban, Doctor-Thesis TU-Darmstadt (2001)
<http://elib.tu-darmstadt.de/diss/000132>
- [12] M. Urban et al., *Nucl. Phys.* A641 (1998) 433
- [13] M. Urban et al., *Nucl. Phys.* A673 (2000) 357
- [14] M. Urban, M. Buballa, J. Wambach, *Phys. Rev. Lett.* 88 (2002) 042002
- [15] G.E. Brown and M. Rho, *Phys. Rev. Lett.* 66 (1991) 2720
- [16] L.A. Kondratyuk et al., *Phys. Rev.* C58 (1998) 1078
- [17] M.F.M. Lutz, Gy. Wolf and B. Friman, *Nuc. Phys.* A706 (2002) 431
- [18] M. Herrmann, B.L. Friman and W. Nörenberg, *Nuc. Phys.* A560 (1993) 411
- [19] R. Rapp, G. Chanfray and J. Wambach, *Nucl. Phys.* A617 (1997) 472
- [20] V.L. Eletsky, M. Belkacem, P.J. Ellis and J.I. Kapusta, *Phys. Rev.* C64 (2001) 035202
- [21] K. Haglin, *Nucl. Phys.* A584 (1995) 719
- [22] R.D. Pisarski, hep-ph/9503330
- [23] G. Wolf, B.Friman and M. Soyeur, *Nucl. Phys.* A640 (1998) 129
- [24] P. Roy et al., *Phys. Rev.* C59 (1999) 2778
- [25] F. Klingl, N. Kaiser and W. Weise, *Nucl. Phys.* A624 (1997) 527
- [26] B. Kämpfer and S. Zschocke, nucl-th/0311042
- [27] T. Hatsuda and S.H. Lee, *Nuc. Phys.* B394 (1993) 221
- [28] S. Leupold, *Phys. Rev.* C64 (2001) 015202
- [29] X. Jin and D.B. Leinweber, *Phys. Rev.* C52 (1995) 3344
- [30] C. Gale and J. Kapusta, *Nucl. Phys.* B357 (1991) 65
- [31] C.L. Korpa and S. Pratt, *Phys. Rev. Lett.* 64 (1990) 1502
- [32] R.A. Schneider and W. Weise, *Phys. Lett.* B515 (2001) 89

- [33] K. Saito, K. Tsushima, A.W. Thomas and A.G. Williams, Phys. Lett. B433 (1998) 243
- [34] M. Wachs, Doctor-Thesis TU-Darmstadt (2000)
<http://elib.tu-darmstadt.de/diss/000050>
- [35] B. Friman, H.J. Pirner, Nucl. Phys. A617 (1997) 496
- [36] G. Baym, Phys. Rev. 127 (1962) 1391
- [37] A.B. Migdal, Rev. Mod. Phys. 50 No. 1 Part 1 (1978), A.B. Migdal, et al., Phys. Rep. 192 (1990) 179
- [38] H. van Hees and J. Knoll, Nuc. Phys. A683 (2001) 369
- [39] L.P. Kadanoff and G. Baym, Quantum statistical Mechanics, Addison Wesley Publishing Comp. (1994)
- [40] Y.B. Ivanov, J. Knoll and D.N.Voskresensky, Nuc. Phys. A657 (1999) 413
- [41] S. Weinberg, Phys. Rev. Lett. 17 (1966) 616
- [42] Y. Tomozawa, Nuov. Cim. A46 (1966) 707
- [43] S. Weinberg, The Quantum Theory of Fields Vol. 1, Cambridge University Press (2000)
- [44] V. Pascalutsa, Phys. Rev. D58 (1998) 096002
- [45] V.F. Dimitriev and T. Suzuki, Nucl. Phys. A438 (1985) 697
- [46] W. Weinhold, Diploma-Thesis TH-Darmstadt (1995)
<http://www.gsi.de/forschung/tp/publications/thesis.html>
- [47] H. van Hees and J. Knoll, Phys. Rev. D65 (2002) 025010, D65 (2002) 105005 and D66 (2002) 025028
- [48] C.L. Korpa and R. Malfliet, Phys. Rev. C52 (1995) 2756
- [49] T. Suzuki, H. Sakai and T. Tasumi, nucl-th/9901097
- [50] M. Nakano, et al., Int. J. Mod. Phys. E 10 (2001) 459
- [51] C.L. Korpa, private communications
- [52] M.F.M. Lutz, Phys. Lett. B552 (2003) 159
- [53] V. Theileis, Diploma-Thesis TH-Darmstadt (1995)
<http://www.gsi.de/forschung/tp/publications/thesis.html>
- [54] M. Gell-Mann, D. Sharp and W.G. Wagner, Phys. Rev. Lett. 8 (1962) 261
- [55] J. Schwinger, Phys. Lett. B24 (1967) 473
- [56] J. Wess and B. Zumino, Phys. Lett. B37 (1971) 95
- [57] E. Witten, Nucl. Phys. B223 (1983) 422
- [58] F. Klingl, N. Kaiser and W. Weise, Z.Phys. A356 (1996) 193
- [59] J. Knoll and D.Voskresensky, Annals of Physics 249 (1996) 532
- [60] J.J. Sakurai, Currents and mesons, Chicago University Press 1969
- [61] F. Klingl, Doctor-Thesis TU-München (1998)
- [62] C.L. Korpa and M.F.M. Lutz, nucl-th/0306063
- [63] F. Klingl, T. Waas and W. Weise, Nucl. Phys. A650 (1999) 299